Optical second harmonic generation from LaAlO₃/SrTiO₃ interfaces with different in-plane anisotropies

Andrea Rubano[1]**, Mateusz Scigaj**[2]**, Florencio Sánchez**[2]**, Gervasi Herranz**[2] **and Domenico Paparo**[3]

[1] Dipartimento di Fisica 'Ettore Pancini', Università di Napoli 'Federico II', Complesso universitario di Monte Sant'Angelo, via Cintia, 80126 Napoli, Italy
[2] Institut de Ciència de Materials de Barcelona (ICMAB-CSIC), Campus UAB, 08193, Bellaterra, Catalonia, Spain
[3] ISASI—Inst. of Applied Sciences and Intelligent Systems, Consiglio Nazionale delle Ricerche, via Campi Flegrei 34, 80078 Pozzuoli, Italy

E-mail: d.paparo@isasi.cnr.it

Abstract

Oxide growth with semiconductor-like accuracy allows the fabrication of atomically precise thin films and interfaces displaying a wide range of phases and functionalities that are absent in the corresponding oxide bulk materials. Among the other properties it was found that a two-dimensional electronic gas is formed under some circumstances at the LaAlO₃/SrTiO₃(0 0 1) interface separating two typical insulating perovskite crystals. The origin of this conducting state has been discussed at length, since different doping mechanisms can act in these material systems. Many experimental results point to the so-called *polar catastrophe* scenario as the principal mechanism driving the formation of the two-dimensional electronic gas. According to this mechanism, the existence of an interfacial polar discontinuity is the key ingredient to drive an electronic reconstruction at the LaAlO₃/SrTiO₃(0 0 1) interface and the consequent formation of a two-dimensional electron gas. This simple picture has been often questioned by the existence of material systems whose interface are predicted being non-polar according to the simplistic 'ionic' limit but that display an electrical behavior analogous to that of LaAlO₃/SrTiO₃(0 0 1) interfaces. This is the case of the LaAlO₃/SrTiO₃(1 1 0), i. e., a LaAlO₃/SrTiO₃ interface with a different in-plane orientation. It is evident that to solve such kind of controversies a detailed investigation of the polar or non-polar state of these interfaces is needed, although this is not simple for the lack of experimental tools that are specifically sensitive to interfacial polarity. Here we apply Optical Second Harmonic Generation to investigate LaAlO₃/SrTiO₃ interfaces with different in-plane orientations to bridge this gap. By comparing our results with recent theoretical findings, we will arrive to the conclusion that the real LaAlO₃/SrTiO₃(1 1 0) interface is strongly polar.

Keywords: surface optical second harmonic generation, LAO/STO interfaces, polarization resolved SHG

(Some figures may appear in colour only in the online journal)

1. Introduction

Since the discovery of a two-dimensional electron gas (2DEG) formed at the interface between the two band insulators LaAlO$_3$ (LAO) and SrTiO$_3$ (STO) [1], a worldwide research effort has unveiled a surprising array of unexpected phenomena in this system, ranging from tunable conductivity to two-dimensional superconductivity [2].

The origin of the interfacial charge carriers in this material system immediately emerged as a highly debated question, since different doping mechanisms can be at play in this oxide heterostructure. A large body of evidence points to the so-called *polar catastrophe* scenario as the mechanism driving the formation of the conducting state [3–10]. According to this picture, in the ideal ionic limit, the LAO/STO(0 0 1) interface is formed by an alternate stacking of $[LaO]^{+1}[AlO_2]^{-1}$ atomic planes over $[SrO]^0[TiO_2]^0$, as displayed in panel (a) of figure 1. As shown in the latter panel this leads to planes with an alternating net charge (σ) that in turn, by using a simple electrostatic model, produces a non-negative electric field ($E_{build-in}$) and hence an electric potential (V) diverging with LAO thickness. For sufficiently thick LAO films, this potential must be relaxed by an interfacial reconstruction. The latter could be ionic, involving lattice distortions and/or some degree of cationic mixing, but it has been proposed that an electronic reconstruction may instead be the dominating effect, involving a transfer of electrons from LAO to STO (see lower part of figure 1(a)), likely into the STO Ti 3d conduction band close to the interface, thus giving rise to the interfacial conduction [3]. This electronic reconstruction then screens $E_{build-in}$ with the generated E_{screen} field as shown in panel (b) of figure 1. On the other hand, the 2DEG is not perfectly localized at the interface, but it spreads along the normal at the interface and creates an inhomogeneous distribution of charges within a very thin interfacial layer d_{polar} [8]. The latter leads to the build up of a strong electric field E^{polar} and the consequent creation of an interfacial quantum well, as shown in figure 1(b).

However, many experimental observations have highlighted the presence of point defects, such as cationic intermixing across the interface or oxygen vacancies, able to introduce a chemical doping even in absence of electronic reconstruction [3, 11–14]. Recently the oxygen-vacancy mechanism has attracted a renewed attention because of the observation that a two-dimensional gas is formed at LAO/STO interfaces even when the LAO film is grown in amorphous phase, so as to rule out polar-discontinuity-related mechanisms [15, 16]. However, while oxygen vacancies may explain the formation of a n-type interface, they can not be used for interpreting the formation of a p-type interface that was predicted since the beginning by the 'polar catastrophe' model and whose elusive nature has for long time puzzled the scientific community. However, very recently, evidences of the formation of a p-type interface have been reported that provide a very strong support to the 'polar catastrophe' model [17].

Another interesting perspective on the 'polar catastrophe' mechanism is represented by a threshold-driven formation of a 2DEG at the LAO/STO(1 1 0) interface, that is an interface formed by depositing LAO atomic layers over (1 1 0)-oriented STO substrates, as shown in panel (a) of figure 2 [18, 19]. According to the same 'ionic' picture, the LAO/STO(1 1 0) interface is formed by a sequence of $[O_2]^{4-}[LaAlO]^{4+}$ planes over $[O_2]^{4-}[SrTiO]^{4+}$ planes that displays no polar discontinuity. To complete this picture the LAO/STO(1 1 1) interface displays a polar discontinuity too, since it is formed by an alternate sequence of $[Al]^{3+}[LaO_3]^{3-}$ over $[Ti]^{4+}[SrO_3]^{4-}$ planes (see panel (b) of figure 2). In fact, this interface shows the same threshold insulator-to-metal transition as the other two interfaces. Additionally, (1 1 0) interfaces allows changing the electronic subband hierarchy with respect to that of (0 0 1) interfaces [20] enabling a distinctive electrostatic gate dependence of 2D superconductivity and Rashba spin–orbit fields [21].

At first sight, this result may appear to challenge the 'polar catastrophe' picture. However, recent theoretical studies show that at the LAO/STO(1 1 0) interface the STO surface is not an ideal stoichiometric surface, but the ground state is characterized by a buckled TiO termination as shown in figure 1(e) of [19]. This predicted ionic structural distortion leads again to an interfacial polar discontinuity, that in turn drives the electronic reconstruction through the same 'polar catastrophe' mechanism described before for the (0 0 1) interface.

In view of all these considerations, an important question arises. Is there an experimental tool suitable to confirm this theoretical prediction, or in other words to probe the existence of a ionic interfacial polarity at the (1 1 0) interface?

In a series of works, [5, 22–30] we have demonstrated that Optical Second Harmonic Generation (SHG) from interfaces is an ideal tool for sensing the interfacial properties of oxide heterostructures. SHG is a nonlinear optical technique based on the detection of doubled-frequency photons in the light reflected or transmitted from the interface. When the illuminated materials are centrosymmetric the SHG is generated with high efficiency only in the thin interfacial regions in which the inversion symmetry is broken. More in general, the source of the interfacial SHG is of two types: 'local' and 'nonlocal' [31]. The 'non-local' or multipolar contribution may rise from a strong electric field gradient due to 'local-field' effects [32]. In the following we will show that multipolar contributions may be safely neglected. On the other hand, a structural reconstruction, as the buckling of Ti ions hypothesized in [19], or a strong electric field as the E^{polar} shown in figure 1(b) may induce or enhance a 'local' SHG or what we name a 'polarity' of the interface. As we will show in the following, both contributions may be globally described by an effective second-order susceptibility tensor, whose strength is then a measure of this interface 'polarity'. After that, the prevalence of one over the other component depends on the specific interface as we will discuss in the following.

An interesting aspect of SHG is that all interfacial electrons, either mobile or localized, may contribute to it. In our previous works on LAO/STO, we have shown that the interfacial polarity, as sensed by SHG, changes dramatically before the onset of conductivity and does not show further variation
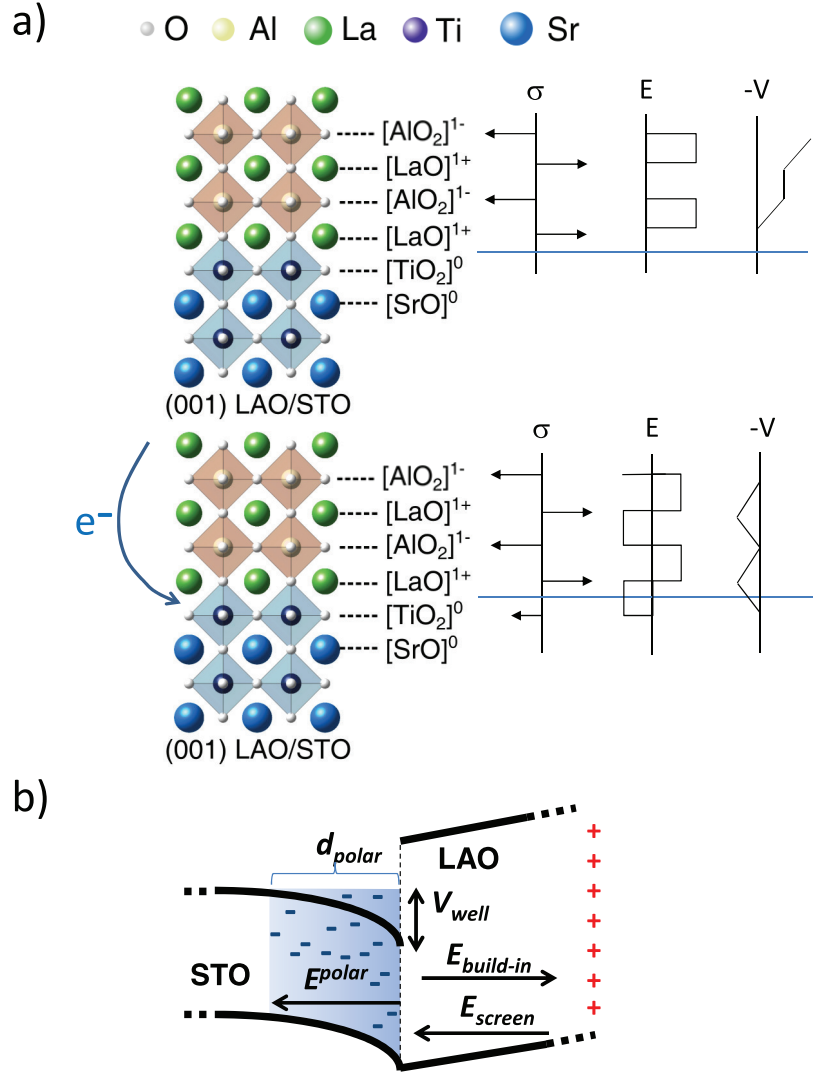
Figure 1. Atomic picture of LAO/STO interface on $(0\,0\,1)$SrTiO$_3$. In panel (a) it is shown a simple electrostatic model explaining the setting up of an electrostatic potential across the LAO film that diverges by increasing the LAO thickness. This potential increase may be avoided through an interfacial reconstruction, either electronic or structural. In panel (b) a band diagram of the LAO/STO interface is reported, illustrating the mechanism of the electronic reconstruction. The latter leads to the build up of an electric field E^{polar} and the consequent formation of a quantum well inside an ultrathin layer of STO.

when the 2DEG forms, thus highlighting the predominant role of charges which are injected at the interface but become localized [5, 22].

In the present work, we have used SHG to analyze the LAO/STO interface in a set of samples with different STO orientations and LAO thicknesses aimed at investigating experimentally the presence or absence of a polar asymmetry at these interfaces, before and/or after the onset of conduction. This is important for a better understanding of the mechanisms acting at these interfaces and leading to their electronic reconstruction. Given the in-plane anisotropy of the LAO/STO(1 1 1) and LAO/STO(1 1 0) interfaces we measure the SHG signal as a function of the linear input and output

light polarization, and as a function of the angle between the incidence plane and the interface principal axis.

2. Theory

In an SHG experiment, the frequency of the incident light is doubled by the interaction with the material. In general this non-linear interaction can be represented by a non-linear term of the polarization $\boldsymbol{P} = \boldsymbol{P}^L + \boldsymbol{P}^{NL}$ induced in the material. This polarization will then be the source of re-emitted light in the wave-equation, according to the Maxwell's equations. Let us neglect the linear term $\boldsymbol{P}^L$, which, in the reflection
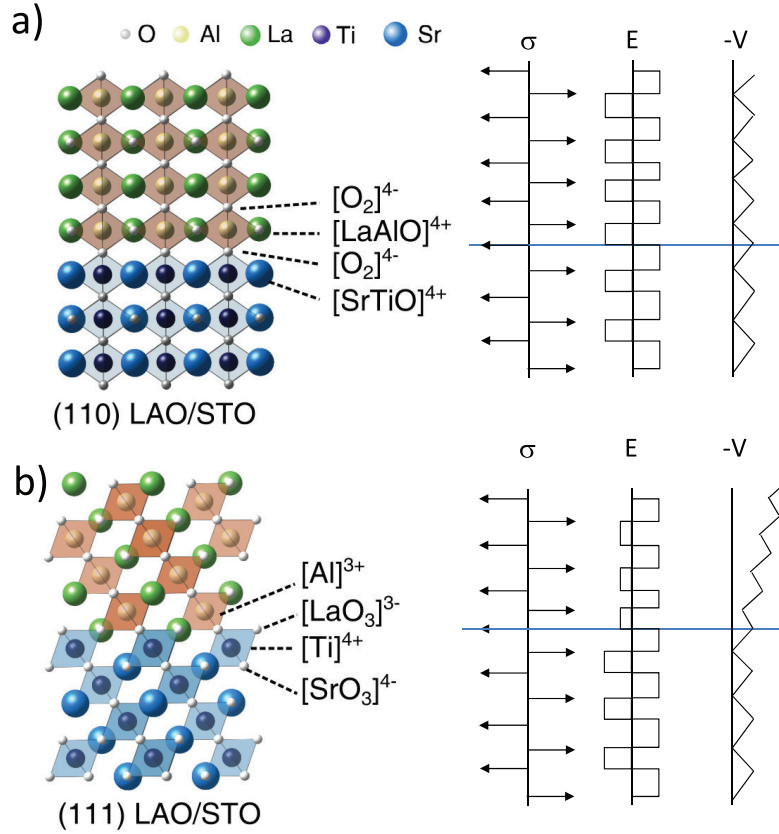
Figure 2. Atomic picture of LAO/STO interface on $(1\,1\,0)$SrTiO$_3$ (a), and $(1\,1\,1)$SrTiO$_3$ (b). In each panel it is shown a simple electrostatic model explaining the absence (a) or the setting up (b) of an electrostatic potential across the LAO film. In the latter case this potential diverges by increasing the LAO thickness as in the case of LAO/STO interface on $(0\,0\,1)$SrTiO$_3$.

geometry used here, just gives the usual reflected light. The non-linear term of the polarization is, in general, a function of the incoming electro-magnetic field. In most cases, it can be expanded in power series. For SHG, the first non-linear term of this series, the quadratic term, is written as:

$$P_i^{NL}(2\omega) = \varepsilon_0 \int \left[\chi_{ijk}^{(2)}(\omega, 2\omega, z) + \chi_{ijkl}^{(3)}(\omega, 2\omega, z) \right.$$
$$\left. \times E_l^{\text{polar}}(0, z) \right] E_j(\omega, z) E_k(\omega, z) \mathrm{d}z, \quad (1)$$

where z is the coordinate along the surface normal, ε_0 is the vacuum dielectric constant, and $\boldsymbol{E}(\omega)$ is the incoming electric field oscillating at ω frequency. The indices (ijk) assume the values of the system coordinates (xyz) and a sum is assumed over repeated indices. In equation (1) $\chi_{ijk}^{(2)}$ and $\chi_{ijkl}^{(3)}$ denote the second- and third-order susceptibility tensors, respectively. The first term takes into account the structural symmetry breaking occurring at the interface between two dissimilar media. The second term describes the symmetry breaking caused by a bias static field, as the one shown in figure 1(b) [33]. These two terms may also account for other contributions, as for instance nonlinear currents induced in the 2DEG.

The relative weight of each of these contributions depends on the specific interface, as we will discuss in the following.

It is easy to show that if the material is inversion symmetric, as the bulks of STO and LAO, the $\chi^{(2)}$ tensor vanishes identically. This implies that in an interface between two centrosymmetric materials and under the dipole approximation, the SHG signal can come *only* from the the polar layer, d_{polar}, where the inversion symmetry is naturally broken. In equation (1) the z integral is extended across the entire thickness of this layer that is assumed much smaller than the optical wavelength. In principle, d_{polar} includes the LAO/STO interface and the LAO surface. Because the LAO film thickness is very small as compared to the optical wavelength, the contribution to SHG of the LAO upper surface would be spatially indistinguishable from the SHG beam generated at the LAO/STO interface and hence this contribution should be taken into account. However, in our past works, [22] we have clearly demonstrated that the source for the SHG signal solely resides in a very thin layer close to the LAO/STO interface and embedded in the STO. This was ascribed to the much wider LAO bandgap and hence to the larger distance of the SHG photon energy from the material resonance. For this reason,

Table 1. Non-vanishing $\widetilde{\chi}^{(2)}$ elements in different symmetries.

Symmetry	Non-vanishing elements
$4mm$ (C_{4v})	xzx = xxz = yyz = yzy
	zxx = zyy
	zzz
$mm2$ (C_{2v})	xzx = xxz
	yyz = yzy
	zxx
	zyy
	zzz
$3m$ (C_{3v})	xzx = xxz = yyz = yzy
	zxx = zyy
	zzz
	yyy = - yxx = -xxy = -xyx

in the following, we will consider as source of the SHG signal exclusively the LAO/STO interface and the STO upper surface in the case of substrates.

If we assume that $\chi_{ijk}^{(2)}(\omega, 2\omega, z)$ and $E_l^{\text{polar}}(0, z)$ have the strongest variation along z compared to the other terms equation (1) becomes

$$P_i^{NL}(2\omega) = \varepsilon_0 \left[\chi_{ijk}^{(2)}(\omega, 2\omega) + \chi_{ijkz}^{(3)}(\omega, 2\omega) V_{\text{well}} \right] E_j(\omega) E_k(\omega), \quad (2)$$

where V_{well} indicates the depth of the potential well as shown in figure 1(b) and we have assumed that $E_l^{\text{polar}}(0, z)$ has only a component along z. The two tensors $\chi_{ijk}^{(2)}(\omega, 2\omega)$ and $\chi_{ijkz}^{(3)}(\omega, 2\omega)$ will have the same azimuthal symmetry. Therefore we group them in an unique tensor $\widetilde{\chi}^{(2)}$. The strength of the latter is a measure of the interface polarity sensed by SHG. In this way, the structural, the electric-field-induced and other contributions become indistinguishable. However, by investigating SHG as a function of in-plane orientation and LAO thickness, we will get some hints on the prevalence of one compared to the other depending on the specific interface.

We remark that we also neglect multipolar contributions to the SHG from the bulk of STO and LAO. We note that these contributions display an in-plane symmetry that is completely different from that of $\widetilde{\chi}^{(2)}$ [34, 35]. This symmetry is often exploited to distinguish these two different SHG sources. As we will show our data agree very well with the in-plane symmetry envisaged for $\widetilde{\chi}^{(2)}$ and hence we conclude that the multipolar terms are negligibly small. For all these reasons we will not consider them further in our analysis.

The $\widetilde{\chi}^{(2)}$ tensor has 27 elements. To exploit the crystal symmetries we first write it in the crystal principal axes (*abc*) coordinate system, where most of the elements are vanishing by symmetry. In absence of structural reconstructions, our three interfaces with (0 0 1), (1 1 0), and (1 1 1) orientations belong to the symmetry groups, $4mm$ (C_{4v} in the Schoenflies notation), $mm2$ (C_{2v}) and $3m$ (C_{3v}), respectively. It is worth noting that structural in-plane reconstructions have been observed at both (1 1 0) and (1 1 1) interfaces [36, 37]. However these

structural reconstructions involve only few atomic cells and hence do not affect the global symmetry of the interface on the macroscopic scale that is probed by SHG.

The non-vanishing terms of $\widetilde{\chi}^{(2)}$ for the three symmetry groups are tabulated in literature [38] and reported for reader's convenience in table 1. It is worth noting that the optical fields in equation (2) are written *inside* the material. We should then write them as a function of the external fields, by resorting to the Fresnel tensor $\widetilde{L}$, that is a two-indices tensor. This tensor couples the transmitted $\boldsymbol{E}_t$ and incident $\boldsymbol{E}_i$ optical fields at the interface according to the following relationship: $\boldsymbol{E}_t = \widetilde{L} \cdot \boldsymbol{E}_i$. For a cubic crystal, as SrTiO$_3$, the Fresnel tensor is diagonal and remains so independently of any applied rotation. Therefore we may write it in the laboratory frame. In that system, it is possible to write the diagonal terms of $\widetilde{L}$ as a function of the input-output angles and the two indices of refraction across the sample surface exposed to air:

$$\begin{cases} L_{xx} = \frac{2n_1 \cos \beta_2}{n_2 \cos \beta_1 + n_1 \cos \beta_2} \\ L_{yy} = \frac{2n_1 \cos \beta_1}{n_1 \cos \beta_1 + n_2 \cos \beta_2} \\ L_{zz} = \frac{2n_1^2 \cos \beta_1}{n_2(n_2 \cos \beta_1 + n_1 \cos \beta_2)} \end{cases}, \quad (3)$$

where β_1 is the incidence angle set in the experiment. n_1 and n_2 are the indices of refraction of air and STO, respectively, the latter depending only on the frequency ω for a given material. In the last sentence an important assumption is implied, i.e. we are treating the interface and the ultrathin LAO layer as being embedded in STO and hence the refractive index of the entire material system is set equal to n_2 (see [22, 25] for a more detailed discussion on this point). The angle β_2 of the transmitted ray is a function of β_1 and the refractive indices $n_{1,2}$ through the Snell law. Therefore, the value of a specific tensor element L_{ii} will depend only on the frequency, which is in our case either ω or 2ω. Therefore, in the following we make use of a simplified notation: $L_{ii}(\omega) = L_{1i}$ and $L_{ii}(2\omega) = L_{2i}$.

By resorting to the Fresnel tensor, we may define an effective $\widetilde{\chi}^{(2)}$ tensor (in the following we will remove the superscript (2) for simplicity) that links the output SHG field to the input optical field and contains all the information about the geometry of the incident and emitted fields. Only the amplitude of the latter will be left outside. The effective $\widetilde{\chi}^{\text{eff}}$ tensor will be than a function of the frequency and the polarization of the incident and emitted light:

$$\chi_{\alpha_{\text{in}}, \alpha_{\text{out}}}^{\text{eff}} = e_{\alpha_{\text{out}}i}^{(2\omega)} L_{2i} \chi_{ijk}(\omega, 2\omega) L_{1j} L_{1k} e_{\alpha_{\text{inj}}}^{(\omega)} e_{\alpha_{\text{in}}k}^{(\omega)}, \quad (4)$$

where $\hat{\boldsymbol{e}}$ are the unit vectors representing the direction of the incoming and outcoming fields and the angles α_{in} and α_{out} the corresponding angles with respect to the p direction, as depicted in figure 3: $\alpha = 0°, 90°, 45°$ correspond to the p, s and d directions, respectively.

The emitted SHG light intensity is proportional to the square modulus of the emitted SHG electric field, and thus it will be in turn proportional to the square modulus of $\widetilde{\chi}^{\text{eff}}$. So, for a given choice of the input and output polarization angles, we measure $|\widetilde{\chi}^{\text{eff}}|^2$ and hence we may extract the elements of $\widetilde{\chi}$. We note that in our measurements we have an arbitrary
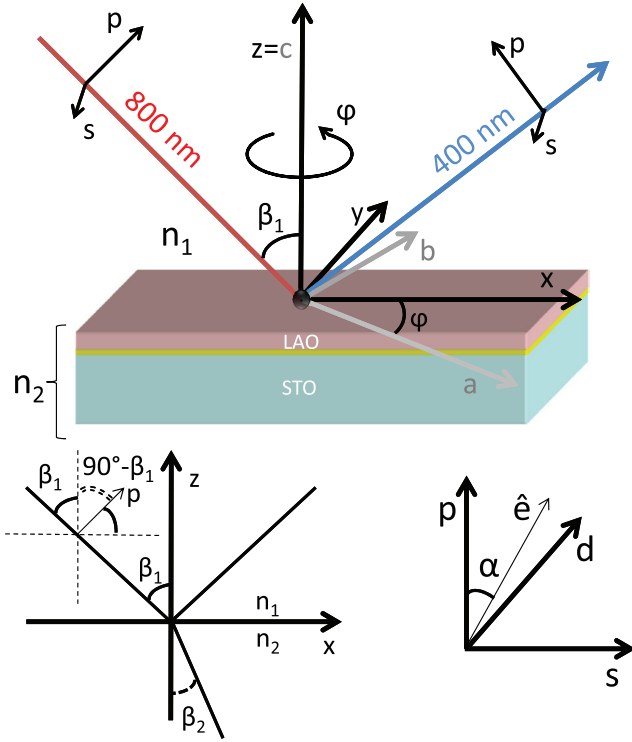
Figure 3. Experimental geometry. The laboratory reference system has *xyz* coordinates, with *xz* incidence plane. The fundamental light has 800 nm wavelength (red line) and the SHG light emitted from the sample has a 400 nm wavelength (blue line). Note that n_1 is the refractive index of air, while n_2 is that of STO and it is assumed to be the same across all the interface and the ultrathin LAO layer (see main text for details on this assumption). The incidence angle is β_1 and the refracted angle into the LAO/STO medium is β_2. The angle ϕ between the laboratory $\hat{x}$ direction and the crystal principal axis $\hat{a}$ may be varied by rotating the sample around the normal to its surface, while different input and output configurations can be set by using a polarizer and an analyzer (made of a half-waveplate plus a polarizer). Here p is the direction parallel to the incident plane, s is parallel to the sample surface and d is at 45° between the two. The general polarization unit-vector $\hat{e}$ forms an angle α with respect to the p direction in the ps plane.

scaling factor (let us call it A), due to the response of the experimental setup. In general, we can write that the measured SHG intensity, I_{SHG}, is given by:

$$I_{\mathrm{SHG}} = A|\widetilde{\chi}^{\mathrm{eff}}|^2. \tag{5}$$

The A factor is the same for all measurements if the experimental geometry, including the beam intensity, is not varied, as we did in our experiment. For this reason, in the following, we will not consider further the parameter A.

According to the geometry sketched in figure 3, we have $\hat{e} = \hat{p}\cos\alpha + \hat{s}\sin\alpha$ for both input and output polarizations. Moreover, for the input polarization we have $\hat{p} = \hat{x}\cos\beta_1 + \hat{z}\sin\beta_1$ and $\hat{s} \equiv \hat{y}$. The same holds for the

output polarizations, but with a reversed sign for the p_x component. Therefore we have:

$$\hat{e}^{\mathrm{in}} = \begin{pmatrix} \cos\alpha_{\mathrm{in}}\cos\beta_1 \\ \sin\alpha_{\mathrm{in}} \\ \cos\alpha_{\mathrm{in}}\sin\beta_1 \end{pmatrix}; \qquad \hat{e}^{\mathrm{out}} = \begin{pmatrix} -\cos\alpha_{\mathrm{out}}\cos\beta_1 \\ \sin\alpha_{\mathrm{out}} \\ \cos\alpha_{\mathrm{out}}\sin\beta_1 \end{pmatrix}. \tag{6}$$

Thus, for the input waves we may write:

$$\widetilde{L}_1 \cdot \hat{e}^{\mathrm{in}} = \begin{pmatrix} L_{1x} & 0 & 0 \\ 0 & L_{1y} & 0 \\ 0 & 0 & L_{1z} \end{pmatrix} \begin{pmatrix} e_x^{\mathrm{in}} \\ e_y^{\mathrm{in}} \\ e_z^{\mathrm{in}} \end{pmatrix}$$

$$= \begin{pmatrix} L_{1x}\cos\alpha_{\mathrm{in}}\cos\beta_1 \\ L_{1y}\sin\alpha_{\mathrm{in}} \\ L_{1z}\cos\alpha_{\mathrm{in}}\sin\beta_1 \end{pmatrix}. \tag{7}$$

For the output waves we obtain an analogous formula by applying the following substitutions $L_1 \rightarrow L_2$, $\alpha_{\mathrm{in}} \rightarrow \alpha_{\mathrm{out}}$, and by changing the sign of the x coordinates.

The elements $\chi^{\mathrm{eff}}_{\alpha_{\mathrm{in}},\alpha_{\mathrm{out}}}$ can be more easily calculated in the crystal reference system. Therefore we rotate the vectors $\widetilde{L}_1 \cdot \hat{e}^{\mathrm{in}}$ and $\widetilde{L}_2 \cdot \hat{e}^{\mathrm{out}}$ in the crystal reference frame and indicate them with $\boldsymbol{R}^{\mathrm{in}}$ and $\boldsymbol{R}^{\mathrm{out}}$, respectively. It is worth noting that in doing this we can leave unchanged the expressions for the Fresnel factors since they are invariant under any rotation. By using the rotated vectors, equation (4) may be rewritten as:

$$\chi^{\mathrm{eff}}_{\alpha_{\mathrm{in}},\alpha_{\mathrm{out}}} = R^{\mathrm{out}}_{\alpha_{\mathrm{out}}i}\chi_{ijk}(\omega,2\omega)R^{\mathrm{in}}_{\alpha_{\mathrm{in}}j}R^{\mathrm{in}}_{\alpha_{\mathrm{in}}k}. \tag{8}$$

In the case of an incidence angle $\beta_1 = 45°$ we may calculate the $\boldsymbol{R}^{\mathrm{in,\ out}}$ elements and obtain the tables 2 and 3.

By substituting the elements of tables 2 and 3 in equation (8) we may find the expression of $\chi^{\mathrm{eff}}_{\alpha_{\mathrm{in}},\alpha_{\mathrm{out}}}$ for different polarization combinations. By exploiting the equality of some components, as reported in table 1, we obtain the following expressions for all the non-vanishing polarization combinations. Some of them are redundant regarding the information they carry on the elements of the $\widetilde{\chi}$ tensor. Therefore, we may choose a set of special polarization combinations that allow to extract all the independent components of $\widetilde{\chi}$. In the section 4 all the sets of chosen combinations for the different symmetries are explicitly reported.

2.1. 4mm symmetry

$$\chi^{\mathrm{eff}}_{ss} = \chi^{\mathrm{eff}}_{ps} = 0$$

$$\chi^{\mathrm{eff}}_{sp} = \frac{1}{\sqrt{2}}L_{2z}L_{1y}^2\chi_{zxx}$$

$$\chi^{\mathrm{eff}}_{ds} = \frac{1}{\sqrt{2}}L_{2y}L_{1y}L_{1z}\chi_{xxz}$$

$$\chi^{\mathrm{eff}}_{pp} = \frac{1}{2\sqrt{2}}L_{2z}L_{1x}^2\chi_{zxx} - \frac{1}{\sqrt{2}}L_{2x}L_{1x}L_{1z}\chi_{xxz} + \frac{1}{2\sqrt{2}}L_{2z}L_{1z}^2\chi_{zzz}. \tag{9}$$

Table 2. Input elements.

$\boldsymbol{R}^{\text{in}}$	p	s	d
x	$\frac{1}{\sqrt{2}}L_{1x}\cos\phi$	$-L_{1y}\sin\phi$	$\frac{1}{2}L_{1x}\cos\phi - \frac{1}{\sqrt{2}}L_{1y}\sin\phi$
y	$\frac{1}{\sqrt{2}}L_{1x}\sin\phi$	$L_{1y}\cos\phi$	$\frac{1}{2}L_{1x}\sin\phi + \frac{1}{\sqrt{2}}L_{1y}\cos\phi$
z	$\frac{1}{\sqrt{2}}L_{1z}$	0	$\frac{1}{2}L_{1z}$

Table 3. Output elements.

$\boldsymbol{R}^{\text{out}}$	p	s	d
x	$-\frac{1}{\sqrt{2}}L_{2x}\cos\phi$	$-L_{2y}\sin\phi$	$-\frac{1}{2}L_{2x}\cos\phi - \frac{1}{\sqrt{2}}L_{2y}\sin\phi$
y	$-\frac{1}{\sqrt{2}}L_{2x}\sin\phi$	$L_{2y}\cos\phi$	$-\frac{1}{2}L_{2x}\sin\phi + \frac{1}{\sqrt{2}}L_{2y}\cos\phi$
z	$\frac{1}{\sqrt{2}}L_{2z}$	0	$\frac{1}{2}L_{2z}$

2.2. mm2 symmetry

$$
\begin{aligned}
\chi_{ss}^{\text{eff}} =&\, 0 \\
\chi_{sp}^{\text{eff}} =&\, \frac{1}{\sqrt{2}} L_{2z} L_{1y}^2 (\chi_{zxx}\sin^2\phi + \chi_{zyy}\cos^2\phi) \\
\chi_{ps}^{\text{eff}} =&\, \frac{1}{2} L_{2y} L_{1x} L_{1z} \sin 2\phi (\chi_{yyz} - \chi_{xxz}) \\
\chi_{ds}^{\text{eff}} =&\, \frac{1}{2} L_{2y} L_{1z} \left[\frac{1}{2} L_{1x}(\chi_{yyz} - \chi_{xxz})\sin 2\phi + \sqrt{2} L_{1y}(\chi_{xxz}\sin^2\phi + \chi_{yyz}\cos^2\phi) \right] \\
\chi_{pp}^{\text{eff}} =&\, -\frac{1}{\sqrt{2}} L_{2x} L_{1x} L_{1z}(\chi_{xxz}\cos^2\phi + \chi_{yyz}\sin^2\phi) + \frac{1}{2\sqrt{2}} L_{2z} L_{1x}^2 (\chi_{zxx}\cos^2\phi + \chi_{zyy}\sin^2\phi) + \frac{1}{2\sqrt{2}} L_{2z} L_{1z}^2 \chi_{zzz}.
\end{aligned}
\tag{10}
$$

2.3. 3m symmetry

$$
\begin{aligned}
\chi_{ss}^{\text{eff}} =&\, L_{2y} L_{1y}^2 \cos 3\phi\, \chi_{yyy} \\
\chi_{sp}^{\text{eff}} =&\, \frac{1}{2} L_{2z} L_{1y}^2 \chi_{zxx} - \frac{1}{\sqrt{2}} L_{2x} L_{1y}^2 \sin 3\phi\, \chi_{yyy} \\
\chi_{ps}^{\text{eff}} =&\, -\frac{1}{2} L_{2y} L_{1x}^2 \cos 3\phi\, \chi_{yyy} \\
\chi_{ds}^{\text{eff}} =&\, \frac{1}{\sqrt{2}} L_{2y} L_{1z} L_{1y} \chi_{xxz} + \left[(L_{1y}^2 - \frac{1}{2} L_{1x}^2)\frac{\cos 3\phi}{2} + \frac{1}{\sqrt{2}} L_{1x} L_{1y} \frac{\sin 3\phi}{\sqrt{2}} \right] L_{2y} \chi_{yyy} \\
\chi_{pp}^{\text{eff}} =&\, \frac{1}{2\sqrt{2}} L_{2x} L_{1x}^2 \sin 3\phi\, \chi_{yyy} + \frac{1}{2\sqrt{2}} L_{2z} L_{1z}^2 \chi_{zzz} + \frac{1}{2\sqrt{2}} L_{2z} L_{1x}^2 \chi_{zxx} - \frac{1}{\sqrt{2}} L_{2x} L_{1x} L_{1z} \chi_{xxz}.
\end{aligned}
\tag{11}
$$

3. Experiment

LAO/STO interfaces of varying thicknesses and substrate orientations were fabricated by pulsed laser deposition (PLD) according to the recipes given in [18, 39]. Two STO substrates, (1 1 0) and (1 1 1) oriented, were used simultaneously for each deposition. The film thickness was monitored by mean of high-pressure Reflection High-Energy Electron Diffraction (RHEED) on the (1 1 0) sample. Films with $n = 4$ and 8 LAO monolayers (MLs) were prepared on STO(1 1 0). At the same time, the simultaneous deposition on STO(1 1 1) leads to ≈5 and ≈10 LAO(1 1 1) MLs. Control samples were also grown in a different deposition run, consisting of 2 and 5 LAO(0 0 1) MLs on STO(0 0 1). The STO(0 0 1) substrates

were chemically and thermally treated to have TiO$_2$ termination [18]. After deposition the samples were cooled down in oxygen rich atmosphere to minimize the formation of oxygen vacancies according to the recipes of [4, 40]. To compare the LAO/STO interfaces and the bare (1 1 0) and (1 1 1) substrates under the same conditions, the latter were exposed to the same temperature and pressure of the deposition process for 1000 s, but without LAO deposition. These samples, and the STO(0 0 1) substrate, are labeled here as $n = 0$ MLs films.

Atomic force microscopy topographic images showed surface morphology of terraces and steps 1 monolayer high, with low root-mean-square roughness of around 1 Å. The transport properties of (1 1 0) and (1 1 1) interfaces were previously characterized by using six-contact arrangement in
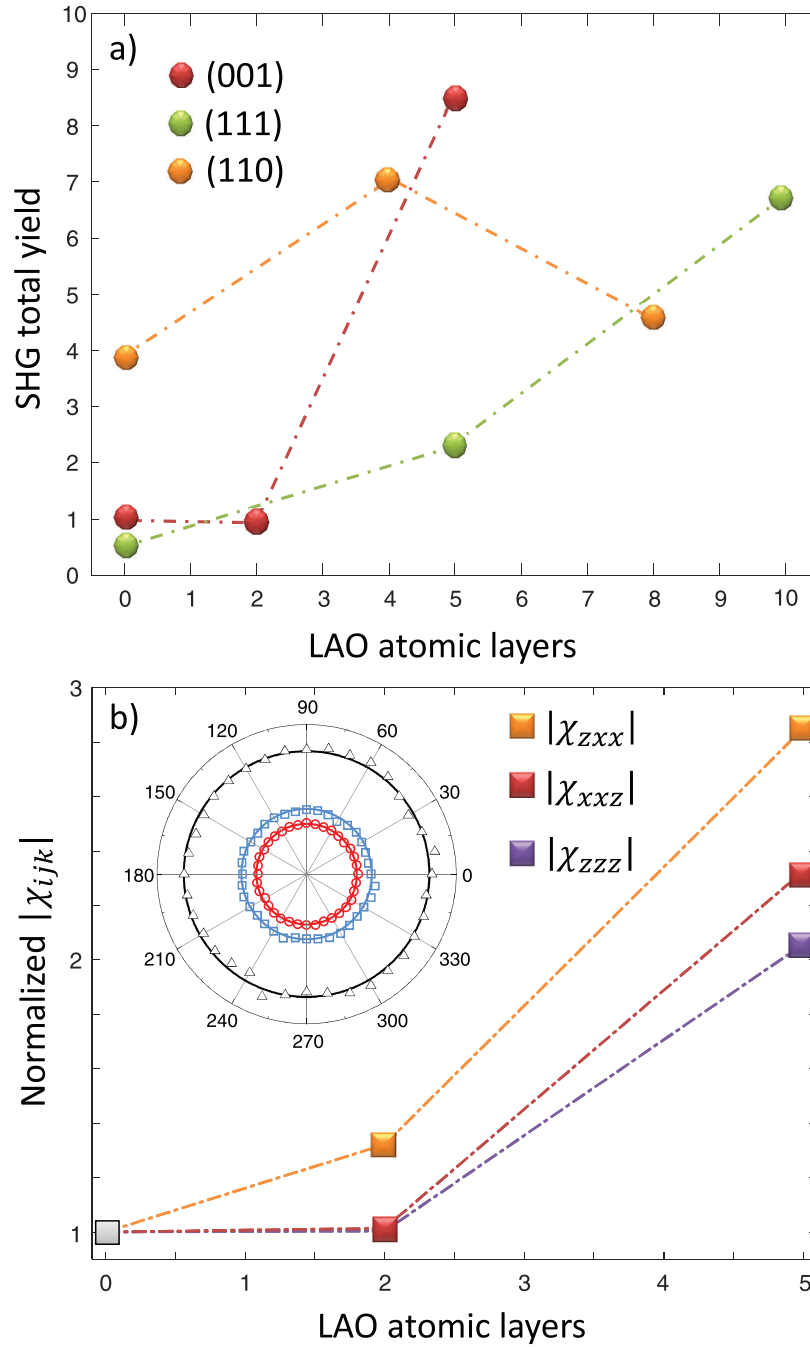
Figure 4. Panel (a) shows the total SHG Yield (integral over all ϕ angles and all polarization combinations) as a function of the LAO coverage. The values are normalized to those measured from the surface of the $(1\,0\,0)$ substrate. Panel (b) shows the $|\chi_{ijk}|$ components for the $(0\,0\,1)$ samples, normalized to their value in the substrate, as a function of the LAO coverage. The inset shows an example of SHG versus azimuthal angle ϕ in the case of a $n = 5$ sample for different polarization combinations: *pp*, black triangles; *ds*, blue squares; *sp*, red circles. As this polar plots do not contain additional information, the data are not shown for all samples.

Hall geometry, from which the sheet resistance and mobility could be extracted, with values similar to those found in $(0\,0\,1)$ interfaces [18]. Similarly to what happens in $(0\,0\,1)$ interfaces, these experiments also indicated the existence of a critical value thickness for a insulator-to-metal transition, with an abrupt jump to a metallic state above a thickness of 7 MLs and 9 MLs for $(1\,1\,0)$ and $(1\,1\,1)$ interfaces, respectively. This observation may suggest that an interface polarity should be associated to both $(1\,1\,0)$ and $(1\,1\,1)$ interfaces, which is further elucidated by our SHG experiments discussed below.

For the optical investigation, the experimental geometry is depicted in figure 3. In particular, the incidence angle, β_1, is set at 45°. Laser pulses of $\approx$35 fs and average energy-per-pulse of 200 μJ were generated at 1 kHz by a Ti:sapphire laser system. The laser wavelength was 800 nm, corresponding to a photon-energy of the fundamental beam of about 1.55 eV and of the second-harmonic of about 3.10 eV, which is far from any optical resonance of both LAO and STO. Both the input fundamental and the output SHG beams were linearly polarized and the polarization direction controlled and analyzed by
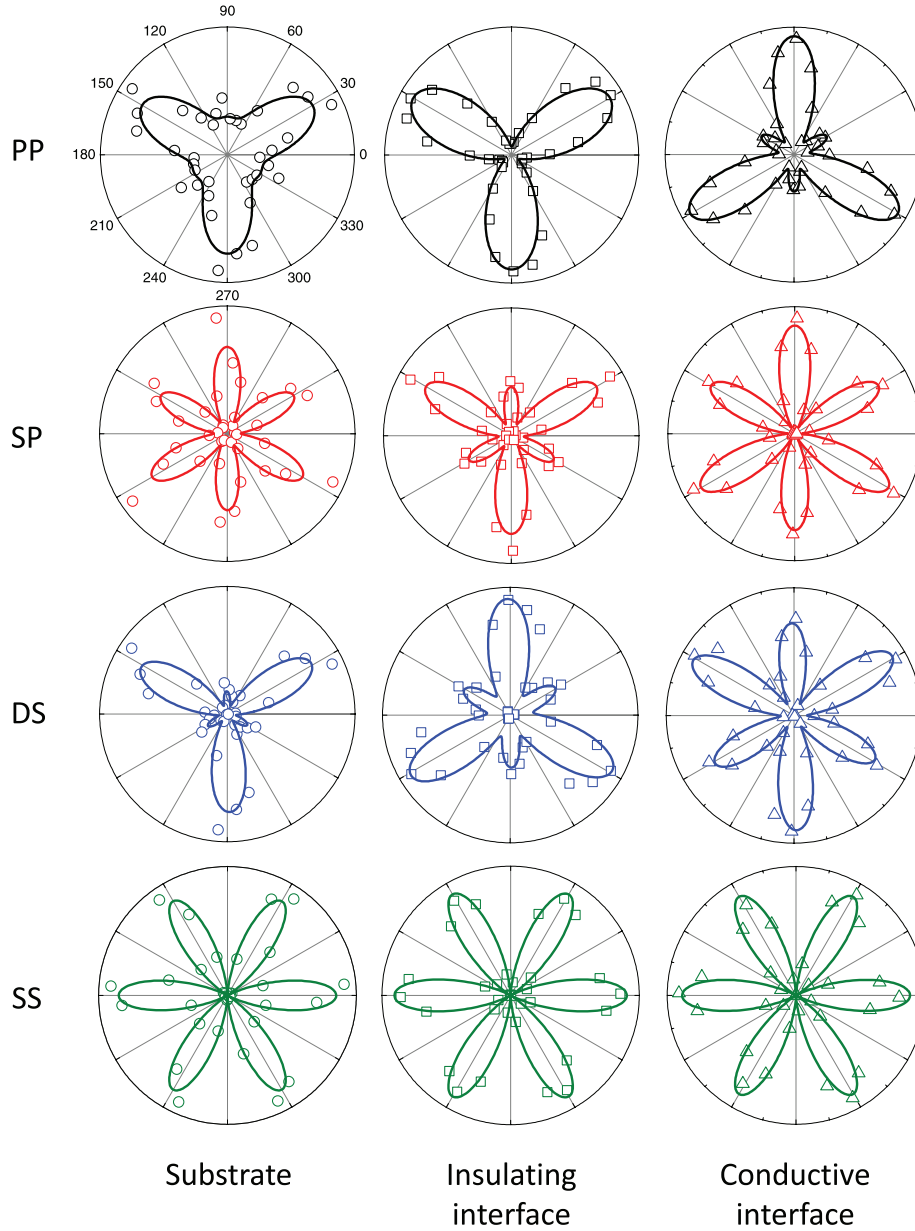
Figure 5. SHG signal as a function of the azimuthal angle ϕ and polarization combinations for (1 1 1) samples. Open symbols are the data and the solid lines are best fit curves according to equation (11).

means of half-waveplates and polarizers. For each sample the experimental conditions were the same. The laser spot size was about 300 μm. The I_{SHG} at different azimuthal angles ϕ was filtered by optical filters and a monochromator from the fundamental light and measured with a photomultiplier. As the photomultiplier saturated by increasing the laser power, the response of our phototube was measured at several signal levels, and a correction curve was derived, so to correct all our data-sets accordingly. All SHG measurements were performed in air.

4. Results and discussion

Let us first observe the total SHG yield as reported in figure 4(a). The total SHG yield is obtained by integrating the

signal over ϕ and averaging on all different polarization configurations. First, we compare the SHG yield for the different substrates. We observe that the signal from the (1 1 0) surface is about four and eight times higher than the signal from the (0 0 1)- and (1 1 1)-STO, respectively. This indicates a strong interface nonlinearity already present at the (1 1 0) surface. Intriguingly, this strong nonlinearity is present in the 4 MLs LAO/STO(1 1 0) sample too and its magnitude is comparable with the above-threshold signals of the other two samples, thus leading to the conclusion that the nonlinearity at this interface is mainly driven by a structural reconstruction. Although from a stoichiometric LAO/STO interface with parallel atomic planes we expect an interface with no-polar discontinuity, a structural reconstruction may lead to an ionic displacement and create off-plane bonds whose nonlinear polarizability
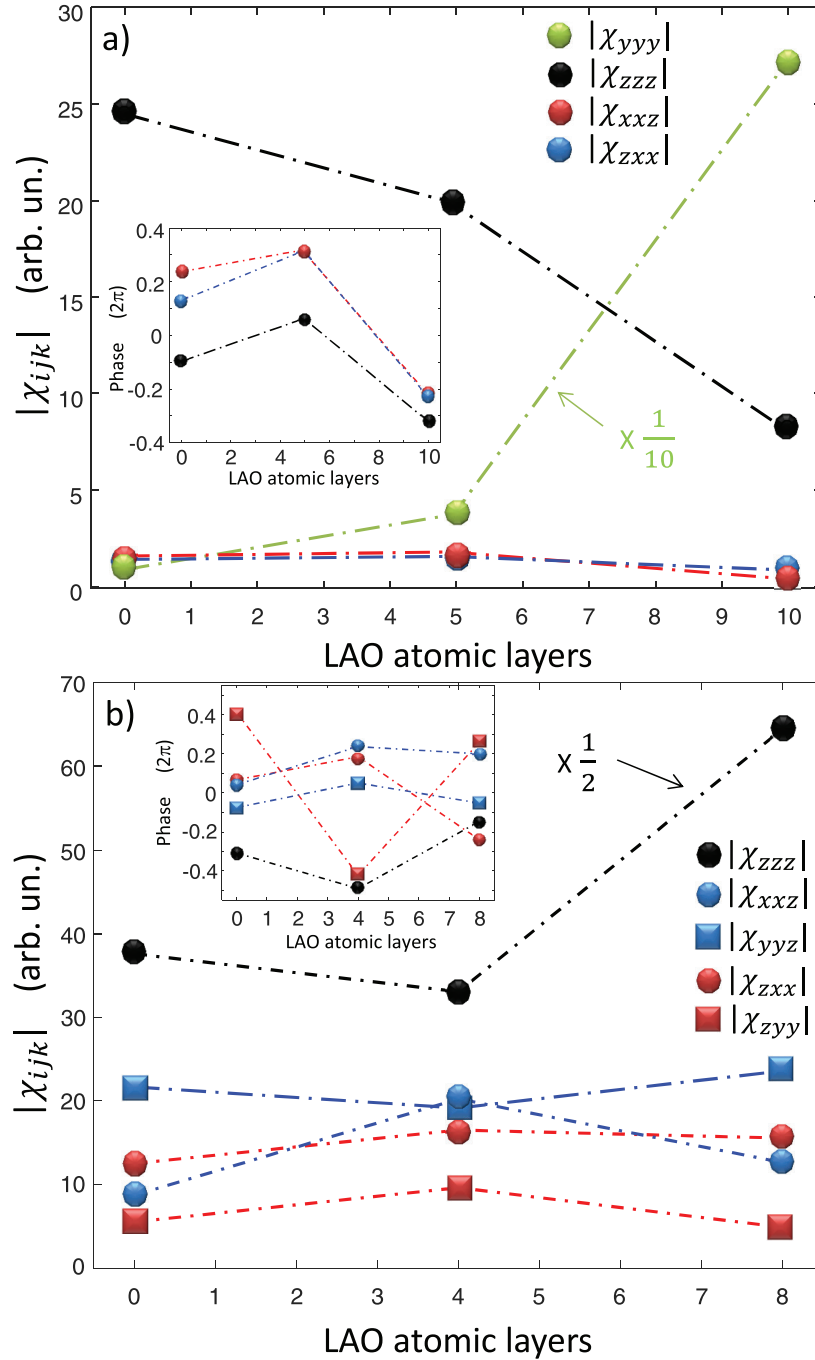
Figure 6. Behavior of the $|\chi_{ijk}|$ elements as a function of LAO coverage for $(1\,1\,1)$ samples (a) and for $(1\,1\,0)$ samples (b). The values of χ_{yyy} in panel (a) and of χ_{zzz} in panel (b) are reduced by a factor 10 and 2, respectively. The values are obtained by means of the fitting procedure as described in the text. The insets show the phase Δ of each element, measured as the angle in a polar representation of the complex $\tilde{\chi}$ elements. The color code used here for the polarization combinations corresponds to that of figures 5 and 7.

enhances the interfacial SHG signal. Therefore, we believe that this result strongly supports the theoretical findings that at the LAO/STO(1 1 0) interface the STO surface is not an ideal stoichiometric surface, but the ground state is characterized by a buckled TiO termination which leads again to an interfacial polar discontinuity [19]. We notice that according to our results this structural distortion is already present on the surface of the bare STO(1 1 0) and that, given the intensity of the SHG signal, the induced polar discontinuity is larger than

those occurring at the other insulating interfaces. To explain this observation it would be desirable to perform theoretical calculations which link the $\tilde{\chi}$ elements to the actual microscopic structure of the interface.

Let us now discuss the behavior of the SHG yield going from an insulating to a conductive interface. Coherently with the findings of our previous works, [5, 22] the SHG from bare STO(0 0 1) and the 2 MLs LAO/STO(0 0 1) interface is approximately constant while it has an abrupt enhancement
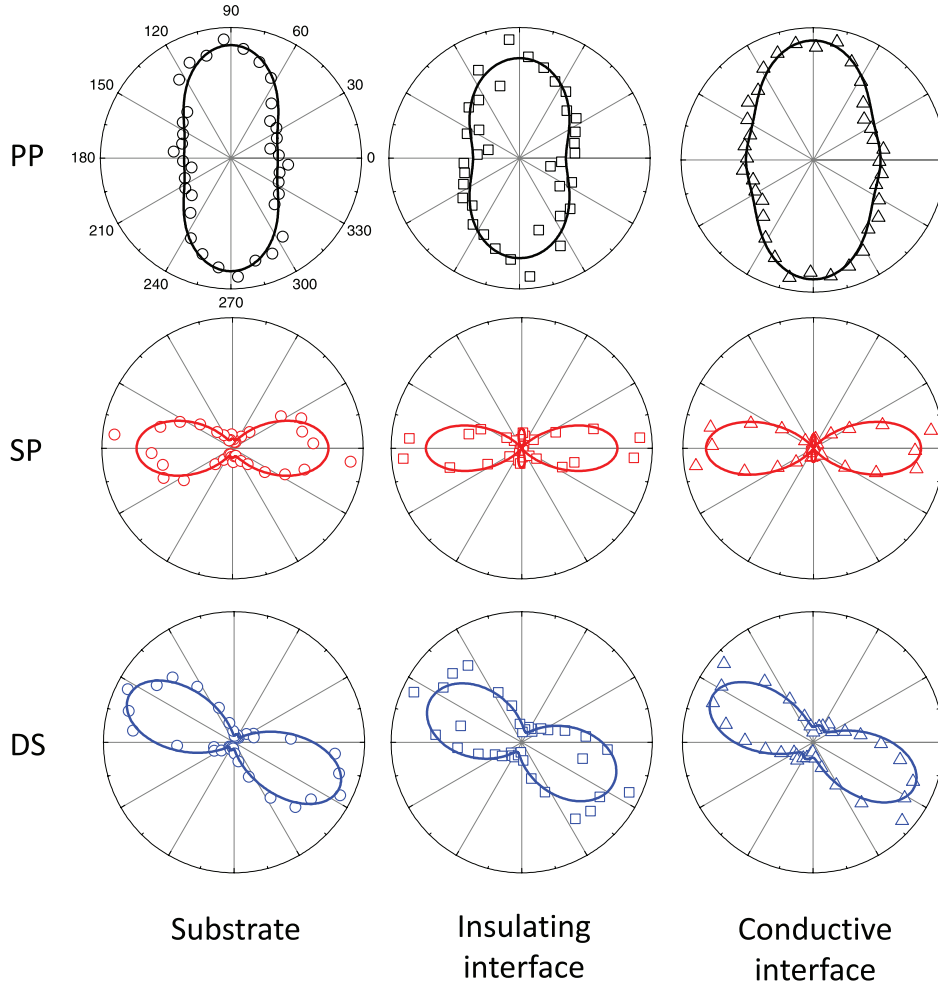
Figure 7. SHG signal as a function of the azimuthal angle ϕ and polarization combinations for (1 1 0) samples. Open symbols are the data and the solid lines are best fit curves according to equation (10).

in the conductive sample ($n = 5$ MLs). This indicates that the polar electric field $\boldsymbol{E}^{\text{polar}}$ set upon charge injection strongly enhances the SHG in the conductive interface. A similar behavior may be observed for the samples grown on (1 1 1) substrates, although there is a significant increase of the signal already in the insulating sample with 5 MLs of LAO, demonstrating that some structural reconstruction occurs in this interface. A systematic study we performed on the LAO/ STO(0 0 1) interface by varying the LAO thickness across the conduction threshold showed that this enhancement of the SHG signal is not correlated to the formation of free carriers, but it is dominated by the injection of charges that become localized [5]. We cannot conclude the same in the case of the LAO/STO(1 1 1) and LAO/STO(1 1 0) since we have not performed the same investigation. In these cases, different contributions (structural, bound, and free electrons) might be comparable and interfere. This might, for instance, explain the slight decrease of the SHG total yield observed in the (1 1 0) conductive interface as compared to the insulating interface.

It is possible that a specific element of the $\tilde{\chi}$ tensor is more sensitive to the SHG contribution coming from a structural symmetry-breaking than other contributions. To scrutinize this hypothesis it is important to extract the different

$\tilde{\chi}$ elements. For this reason now we focus our attention on the SHG signal as a function of polarization and azimuthal angle in order to single out all the elements of the $\tilde{\chi}$ tensor for each interface. As predicted by equation (9), the SHG signal from the (0 0 1) interfaces does not depend on the azimuthal angle for all the polarization combinations. This is nicely confirmed by the inset of figure 4(b) which shows exemplarily a measurement for the $n = 5$ MLs sample at different polarization combinations. As obvious from the second and third of equation (9), we may extract the amplitude of χ_{xxz} and χ_{zxx} by measuring the SHG signal for the *ds* and *sp* polarization combinations, respectively. These two quantities may be used in the last of equation (9) for extracting χ_{zzz}, once the relative phase of these elements is known. This has been done in [22], where we found that $\chi_{xxz}, \chi_{zxx}, \chi_{zzz}$ are always real, with the notable exception of the $n = 1$ MLs sample, and that the χ_{xxz} component has opposite sign (-1) compared to χ_{zxx} and χ_{zzz}. Based on the same assumptions here, we extract the $\tilde{\chi}$ elements shown in figure 4(b).

We observe that all the $\tilde{\chi}$ elements display a strong variation of the SHG signal across the insulator-to-metal transition, going from the under to the above threshold samples, coherently with our previous works.

Let us now discuss the $(1\,1\,1)$ samples. Figure 5 shows all the measurements for *pp*, *sp*, *ss*, and *ds* polarization combinations for $n = 0, 5, 10$ samples. Beside the technical details, let us remark some qualitative evidence. First of all, the average SHG signal is definitely changing a lot with the LAO coverage for the $(1\,1\,1)$ samples, as already observed. Second, the *ss* curves are not much different at $n = 0, 5, 10$, although they have a completely different amplitude as shown below. They all have the same shape, with six equivalent lobes. The other curves, on the contrary, show dramatic changes in the shape by varying the film thickness. In figure 5 the solid lines represent the results of a fitting procedure based on equation (11). The good agreement of the data with the fitting curves confirms that possible multipolar bulk contributions to SHG are negligibly small. The fitting procedure we use is quite straightforward and provide results that are robust against a change in the initial parameters. However, contrary to the $(0\,0\,1)$ samples, there is no way to fit our data by using real quantities for the elements of the $\tilde{\chi}$ tensor, that hence we assume complex. The latter might be a further indication that different contributions with different optical phases act and interfere in these samples, while we have strong evidences that in $(0\,0\,1)$ samples the interface nonlinearity is mainly driven by bound electrons. We first recognize that the *ss* combination depends on χ_{yyy} only, thus it is possible to obtain directly χ_{yyy} up to an unknown phase factor. Then we fix the so obtained value of χ_{yyy} in the equation (11) for *sp* and *ds*, where only χ_{zxx} and χ_{xxz}, respectively, are left as adjustable parameters.

As said it is not possible to measure the phase of the χ_{yyy} component, as it only appears in square modulus. Therefore the phases of χ_{zxx} and χ_{xxz} may be obtained only as relative values with respect to the χ_{yyy} phase. Finally, all components are participating in the last of equation (11) describing the *pp* combination, so that we can extract the χ_{zzz} component by fixing all the others to the previously extracted values.

In figure 6(a) the results of the fitting procedure are summarized as a function of the LAO coverage. We notice that all components are changing, but the χ_{yyy} has the largest change of all: it becomes about 30 times higher above threshold than its value below threshold. It is interesting to note that the χ_{zzz} value of the substrate is larger than that of χ_{yyy}, but above threshold the latter becomes huge compared to χ_{zzz}. This is surprising since in $(0\,0\,1)$ samples χ_{zzz} is usually the largest component. Moreover the χ_{zzz} element decreases quite a lot with the LAO coverage, a reduction of about 70%, and the same happens to χ_{zxx} and χ_{xxz}. As a final remark, the phases shown in the inset of figure 6(a) also changes dramatically, undergoing a rotation of more than π in the 10 MLs sample.

An analogous fitting procedure has been applied to the data from $(1\,1\,0)$ samples. Figure 7 shows all the measurements for *pp*, *sp*, and *ds* combinations on $n = 0, 4, 8$ LAO/STO samples, and the best-fit curves obtained by means of equation (10). We remark that equation (10) predict a vanishing signal for the *ss* combination, as we have observed experimentally, while this is not the case if a bulk multipolar contribution is significant [35]. This observation together with the good agreement of the data with the fitting curves confirms the absence

of a multipolar bulk contribution to SHG. We note that these polarization combinations carry all the information on the $\tilde{\chi}$ tensor elements, although, for completeness, we report in the equation (10) all the non-vanishing polarization combinations for the $(1\,1\,0)$ interfaces. The fit results are summarized in figure 6(b) as a function of the LAO coverage. In Fig 7, despite the insulator-to-metal transition, no qualitative change is immediately visible in the measurements. Beside some numerical change, the overall shape of the curves is quite unchanged. On the contrary, the behavior of the $\tilde{\chi}$-components as a function of the LAO coverage shows interesting trends. In particular, while all the other components are approximately constant over the entire range of thicknesses, the χ_{zzz} component increases by about 50% across the insulator-to-metal transition. The phases reported in the inset of figure 6(b) show a pretty irregular behavior, for which, at the moment, we do not have a sound explanation. A possible interpretation is that different contributions (structural, free and bound electrons) whose relative weight changes below and above the conduction threshold have tensor elements with different phases, among the tensor elements of the same interface as well as different interfaces.

By gathering together the results on the SHG yield (figure 4(a)) and the χ_{zzz}-component of the $(1\,1\,0)$ samples, it is clear that these samples display a strong interfacial polarity already below the conduction threshold, thus confirming the theoretical results reported in [19]. Moreover, the behavior of the χ_{zzz}-component shows that the interface nonlinearity is also affected somehow by the the charge injection. Why charge injection modifies only this component is an interesting issue as well as the irregular behavior of the phase factor observed in figure 6(b) and the large SHG observed already at the STO$(1\,1\,0)$ surface. All these experimental observations deserve a more detailed theoretical investigation suitable to link the $\tilde{\chi}$-components to the interface microscopic structure. However, this investigation is beyond the scope of the present work.

5. Conclusions

In summary we have investigated LAO/STO interfaces with different STO orientations and LAO thicknesses by means of optical second harmonic generation that once more has revealed being an invaluable tool for probing the interface properties of the LAO/STO heterostructures. Despite the ionic model with a stoichiometric structure that foresees a polar discontinuity only in $(0\,0\,1)$ and $(1\,1\,1)$ samples, we find that $(1\,1\,0)$ interface undergoes a strong structural reconstruction, already large at the surface of bare STO$(1\,1\,0)$. We believe that our results confirm recent theoretical findings highlighting the formation of a buckled TiO termination, which is energetically favored against a polar stoichiometric STO interface and which results in an interfacial polar discontinuity. This structural distortion of the interface is already present in the bare substrate and it is reflected in our observation of a strong SHG signal from these interfaces. Therefore, our results support the idea of the presence of a strong polar discontinuity at the

(1 1 0) interface too. Moreover, by analyzing in detail the elements of the $\tilde{\chi}$ tensor, we find that while in LAO/STO(0 0 1) samples all the $\tilde{\chi}$-components are influenced by the charge injection occurring above threshold, for the other orientations, only some components show a strong variation across the insulator-to-metal transition. For a better understanding of the latter findings a detailed theoretical work is needed that is suitable to link the microscopic structure of the interface to the elements of the $\tilde{\chi}$ tensor. This is a very difficult task that goes beyond the scope of the present work.

Acknowledgments

ORCID iDs

Domenico Paparo https://orcid.org/0000-0002-7745-230X

References

[1] Ohtomo A and Hwang H Y 2004 A high-mobility electron gas at the LaAlO$_3$/SrTiO$_3$ heterointerface *Nature* **427** 423

[2] Granozio F M, Koster G and Rijnders G 2013 Functional oxide interfaces *MRS Bull.* **38** 1017–23

[3] Nakagawa N, Hwang H Y and Muller D A 2006 Why some interfaces cannot be sharp *Nat. Mater.* **5** 204

[4] Thiel S, Hammerl G, Schmehl A, Schneider C W and Mannhart J 2006 Tunable quasi-two-dimensional electron gases in oxide heterostructures *Science* **313** 1942

[5] Savoia A *et al* 2009 Polar catastrophe and electronic reconstructions at the LaAlO$_3$/SrTiO$_3$ interface: evidence from optical second harmonic generation *Phys. Rev.* B **80** 075110

[6] Reinle-Schmitt M L *et al* 2012 Tunable conductivity threshold at polar oxide interfaces *Nat. Commun.* **3** 932

[7] Cancellieri C *et al* 2011 Electrostriction at the LaAlO$_3$/SrTiO$_3$ interface *Phys. Rev. Lett.* **107** 056102

[8] Cantoni C *et al* 2012 Electron transfer and ionic displacements at the origin of the 2D electron gas at the LAO/STO interface: direct measurements with atomic-column spatial resolution *Adv. Mater.* **24** 3952

[9] Liu Z Q *et al* 2013 Origin of the two-dimensional electron gas at LaAlO$_3$/SrTiO$_3$ interfaces: the role of oxygen vacancies and electronic reconstruction *Phys. Rev.* X **3** 021010

[10] Gazquez J, Stengel M, Mishra R, Scigaj M, Varela M, Roldan M A, Fontcuberta J, Sanchez F and Herranz G 2017 Competition between polar and nonpolar lattice distortions in oxide quantum wells: new critical thickness at polar interfaces *Phys. Rev. Lett.* **119** 106102

[11] Pauli S A and Willmott P R 2008 Conducting interfaces between polar and non-polar insulating perovskites *J. Phys.: Condens. Matter.* **20** 264012

[12] Yoshimatsu K, Yasuhara R, Kumigashira H and Oshima M 2008 Origin of metallic states at the heterointerface

between the band insulators LaAlO$_3$ and SrTiO$_3$ *Phys. Rev. Lett.* **101** 026802

[13] Kalabukhov A S *et al* 2009 Cationic disorder and phase segregation in LaAlO$_3$/SrTiO$_3$ heterointerfaces evidenced by medium-energy ion spectroscopy *Phys. Rev. Lett.* **103** 146101

[14] Chambers S A *et al* 2010 Instability, intermixing and electronic structure at the epitaxial LaAlO$_3$/SrTiO$_3$(0 0 1) heterojunction *Surf. Sci. Rep.* **65** 317

[15] Chen Y Z, Pryds N, Kleibeuker J E, Koster G, Sun J R, Stamate E, Shen B G, Rijnders G and Linderoth S 2011 Metallic and insulating interfaces of amorphous SrTiO$_3$-based oxide heterostructures *Nano Lett.* **11** 3774–8

[16] Lee S W, Liu Y Q, Heo J and Gordon R G 2012 Creation and control of two-dimensional electron gas using Al-based amorphous Oxides/SrTiO$_3$ heterostructures grown by atomic layer deposition *Nano Lett.* **12** 4775–83

[17] Lee H *et al* 2018 Direct observation of a two-dimensional hole gas at oxide interfaces *Nat. Mater.* **17** 231–6

[18] Sánchez F, Ocal C and Fontcuberta J 2014 Tailored surfaces of perovskite oxide substrates for conducted growth of thin films *Chem. Soc. Rev.* **43** 2272–85

[19] Annadi A *et al* 2013 Anisotropic two-dimensional electron gas at the LaAlO$_3$/SrTiO$_3$ (1 1 0) interface *Nat. Commun.* **4** 1838

[20] Pesquera D *et al* 2014 Two-dimensional electron gases at LaAlO$_3$/SrTiO$_3$ interfaces: orbital symmetry and hierarchy engineered by crystal orientation *Phys. Rev. Lett.* **113** 156802

[21] Herranz G *et al* 2015 Engineering two-dimensional uperconductivity and Rashba spin–orbit coupling in LaAlO$_3$/SrTiO$_3$ quantum wells by selective orbital occupancy *Nat. Commun.* **6** 6028

[22] Rubano A *et al* 2011 Spectral and spatial distribution of polarization at the LaAlO$_3$/SrTiO$_3$ interface *Phys. Rev.* B **83** 155405

[23] Günter T *et al* 2012 Spatial inhomogeneities at the LaAlO$_3$/SrTiO$_3$ interface: evidence from second harmonic generation *Phys. Rev.* B **86** 235418

[24] Rubano A, Günter T, Fink T, Paparo D, Marrucci L, Cancellieri C, Gariglio S, Triscone J-M and Fiebig M 2013 Influence of atomic termination on the LaAlO$_3$/SrTiO$_3$ interfacial polar rearrangement *Phys. Rev.* B **88** 035405

[25] Paparo D, Rubano A and Marrucci L 2013 Optical second-harmonic generation selection rules and resonances in buried oxide interfaces: the case of LaAlO$_3$/SrTiO$_3$ *J. Opt. Soc. Am.* B **30** 2452

[26] Rubano A, Aruta C, di Uccio U S, Granozio F M, Marrucci L, Günter T, Fink T, Fiebig M and Paparo D 2013 Electronic states at polar/nonpolar interfaces grown on SrTiO$_3$ studied by optical second harmonic generation *Phys. Rev.* B **88** 245434

[27] De Luca G, Rubano A, di Gennaro E, Khare A, Granozio F M, di Uccio U S, Marrucci L and Paparo D 2014 Potential-well depth at amorphous-LaAlO$_3$/crystalline-SrTiO$_3$ interfaces measured by optical second harmonic generation *Appl. Phys. Lett.* **104** 261603

[28] Rubano A, Günter T, Lilienblum M, Aruta C, Miletto Granozio F, Scotti di Uccio U, Marrucci L, Paparo D and Fiebig M 2015 Optical second harmonic imaging as a diagnostic tool for monitoring oxides thin-film epitaxial growth *App. Surf. Sci.* **327** 413–7

[29] Rubano A, De Luca G, Schubert J, Wang Z, Zhu S, Schlom D G, Marrucci L and Paparo D 2015 Polar asymmetry of La$_{(1-\delta)}$Al$_{(1+\delta)}$O$_3$/SrTiO$_3$ heterostructures probed by optical second harmonic generation *Appl. Phys. Lett.* **107** 101603

[30] Rubano A, Günter T, Fiebig M, Granozio F M, Marrucci L and Paparo D 2018 Ultrafast modification of the polarity at LaAlO$_3$/SrTiO$_3$ interfaces *Phys. Rev.* B **97** 035438

[31] Guyot-Sionnest P and Shen Y R 1987 Local and nonlocal surface nonlinearities for surface optical second-harmonic generation *Phys. Rev.* B **35** 4420–6

[32] Mendoza B S and Mochán W L 1996 Local-field effect in the second-harmonic-generation spectra of Si surfaces *Phys. Rev.* B **53** R10473

[33] Aktsipetrov O A, Fedyanin A A, Melnikov A V, Dadap J I, Hu X F, Anderson M H, Downer M C and Lowell J K 1997 D.c. electric field induced second-harmonic generation spectroscopy of the Si(0 0 1)-SiO$_2$ interface: separation of the bulk and surface non-linear contributions *Thin Solid Films* **294** 231–4

[34] Lüpke G 1999 Characterization of semiconductor interfaces by second-harmonic generation *Surf. Sci. Rep.* **35** 75–161

[35] Omote M, Kitaoka H, Kobayashi E, Suzuki O, Aratake K, Sano H, Mizutani G, Wolf W and Podloucky R 2005 Spectral, tensor, and *ab initio* theoretical analysis of optical second harmonic generation from rutile TiO$_2$(1 1 0) and (0 0 1) faces *J. Phys.: Condens. Matter* **17** S175–200

[36] Russell B C and Castell M R 2008 Reconstructions on the polar SrTiO$_3$ (1 1 0) surface: analysis using STM, LEED, and AES *Phys. Rev.* B **77** 245414

[37] Torrelles X, Cantele G, De Luca G M, Di Capua R, Drnec J, Felici R, Ninno D, Herranz G and Salluzzo M 2019 Electronic and structural reconstructions of the polar (1 1 1) SrTiO$_3$ surface *Phys. Rev.* B **99** 205421

[38] Boyd R W 1992 *Nonlinear Optics* (New York: Academic) p 44

[39] Bachelet R, Valle F, Infante I C, Sánchez F and Fontcuberta J 2007 Step formation, faceting and bunching in atomically flat SrTiO$_3$ (1 1 0) surfaces *Appl. Phys. Lett.* **91** 251904

[40] Sing M *et al* 2009 Profiling the interface electron gas of LaAlO$_3$/SrTiO$_3$ heterostructures with hard x-ray photoelectron spectroscopy *Phys. Rev. Lett.* **102** 176805